
DOI: 10.1002/chem.201202608

Communication

D.[^]S. Su et[^]al.

Pd Nanoparticles in Acetylene-Selective Hydrogenation

Improved Selectivity by Stabilizing and Exposing Active Phases on Supported Pd Nanoparticles in Acetylene-Selective Hydrogenation

Dr. Lidong Shao,^[a] Dr. Bingsen Zhang,^[a,b] Dr. Wei Zhang,^[a] Dr. Detre Teschner,^[a] Dr. Frank Girgsdies,^[a] Prof.[^]Dr. Robert Schlögl,^[a] and Dr. Dang Sheng Su^{*[a,b]}

^[a] Department of Inorganic Chemistry
Fritz Haber Institute of the Max Planck Society
Faradayweg 4--6, 14195 Berlin (Germany)
Fax: (+49)[^]30-8413-4401
E-mail: dangsheng@fhi-berlin.mpg.de

^[b] Shenyang National Laboratory for Materials Science
Institute of Metal Research, Chinese Academy of Sciences
72 Wenhua Road, 110016 Shenyang (P.R. China)

 Supporting information for this article is available on the WWW under
<url><http://dx.doi.org/10.1002/chem.201202608></url>.

Palladium dynamics: . Under hydrogenation conditions, saturating over-active palladium by carbon diffusion permits a stable and selective particle surface. By choosing supports with suitable geometric structures and establishing a strong interaction between supports and metal particles, accumulated species can be regularly rearranged and reaction-selective phase can be exposed.

<?><?>text ok?<?><?>

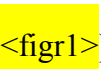
Supported Catalysts


acetylene
electron microscopy
hydrogenation
nanotubes
supported catalysts

Palladium-catalyzed selective hydrogenation of acetylene has been one of the most studied hydrogenation reactions in the last century.^[1,^2] Despite its long-term application in pharmaceuticals and polyethylene synthesis, kinetic studies revealing active centers are hindered, because palladium undergoes dynamic changes,^[3] and reaction-created intermediates continuously interact with Pd and its support to form an active complex during reactions.^[4] For example, Pd carbide (PdC_x), formed by diffusing decomposed carbon into a Pd lattice commonly in its saturation phase, has long been reported during Pd-catalyzed acetylene hydrogenations.^[3--8] Carbonaceous deposition, another important species generated and accumulated on Pd and support surfaces, reportedly influences selective hydrogenations by affecting hydrogen diffusions.^[9--12] In addition, the strong metal--support interaction (the SMSI effect) may affect reactions for supported Pd catalysts through electronically and geometrically arranging active species.^[13,^14] As consequence of various active species on Pd and its support, competitions between reaction formed phases (PdC_x , PdH_y , and deposited species) are temperately responsible for the reaction pathway, but the equilibrium constantly changes, as long as metallic Pd exists in a catalytic system.

The present work aims to develop a methodology to simplify reaction pathways and discriminate the active phase by stabilizing reaction-induced modifications during reactions. Herein, this means completely transforming the Pd metallic phase into a thermally stable PdC_x phase starting from the beginning of acetylene hydrogenation. In addition, the SMSI effect was investigated with Pd on different supports to examine the possibility of regularly exposing the stabilized active phase during the reaction. Pd-phase transformation and stabilization were studied by using an in situ technique; modified catalyst morphology was investigated by using microscopic tools. A rational design of exposing the stabilized active

phase (saturated PdC_x) on various supports was later confirmed in acetylene-hydrogenation flow-reactor conditions.

First, in situ X-ray photoelectron spectroscopy (XPS) was applied to study the influences of particle size and supporting materials on the surface and subsurface electronic properties of Pd-based samples under reaction conditions. Pd supported on carbon nanotubes (Pd/CNTs, 4.3 wt% Pd) was investigated and compared with Pd foil, which was reported in our previous work.^[3] We characterized the state after storing the "as is" sample in air, as well as under acetylene hydrogenation conditions. Detailed experimental parameters are specified in the Supporting Information. The Pd 3d core level shows three contributions in the as-prepared state, with 5/2 spin-orbit components at 335.0, 335.6, and 337.5 eV (Figure¹ .

The latter (337.5 eV) can be assigned to some oxidized Pd clusters on CNTs.^[15] The 335.0 eV peak is characteristic of metallic Pd, whereas the 335.6 eV peak is characteristic of the carbon-diffused PdC_x surface phase.^[4,16] Herein, the partial occurrence of PdC_x on as-prepared Pd/CNTs is possibly a result of the strong metal/support interaction established during sample preparations. As the reactant gas mixture flowed in with heat, the metallic component (Pd) underwent a phase transformation under acetylene hydrogenation and formed an intensive PdC_x peak (see Figure¹ , as was observed for unsupported Pd foil in our previous report.^[3] During hydrogenation over Pd/CNTs, the product evolution was followed by MS, which showed that at 393 K ethylene was preferentially formed (Figure^{S1} in the Supporting Information), consistent with enhanced selectivity over an unsupported Pd foil.^[3] The appearance of PdC_x on both Pd/CNTs (Pd particle size distribution was about 7 nm) and unsupported Pd foil under hydrogenation suggests that the carburization process, that is, diffusing carbon into the Pd lattice on surface areas, is not affected by particle size and supporting materials.

Although surface and subsurface PdC_x have recently been considered as active phases controlling selectivity during alkyne hydrogenation,^[3,4] its thermal stability governed by saturation degree (diffused carbon concentration) has not been discussed specifically as a role of affecting reactions. As a consequence, unsaturated PdC_x may lead to a co-existence of

PdC_xH_y and deviates the reaction from selective directions.^[3,4,6,7] Therefore, physical recognition of surface and subsurface PdC_x to bulk PdC_x is crucial, because the carbon concentration of PdC_x on surface area is determined by the carburization degree of the entire Pd particle.

To obtain bulk-phase PdC_x information, in situ X-ray diffraction (XRD) was conducted. Structural analyses were carried out on Pd/CNTs and compared with commercially available Pd/ Al_2O_3 (5 wt% Pd) for carburization studies. In the case of the Pd/ Al_2O_3 catalyst (Figure 2a), switching on hydrogen (4%, rest in helium) at room temperature formed Pd hydride (PdH_x) with expanded lattice constants indexed by shifted peaks, which matches the physical description of palladium hydride that PdH_x (with $x < 1$) is the metallic palladium contained a substantial quantity of hydrogen within its crystal lattice. Switching back to He caused PdH_x to decompose and restored the Pd metallic phase (Figure S2 in the Supporting Information). Then, repetitive fast XRD scans (ca. 7–8 min per scan) covering the Pd 111 peak ($2\theta = 36\text{--}42^\circ$) were executed while introducing acetylene into the feed in the presence of H_2 (2% C_2H_2 , 4% H_2 , rest in He in total flow of 100 mL min⁻¹). Interestingly, PdH_x formation was prohibited at room temperature (Figure S3 in the Supporting Information). Afterward, increasing the temperature to 393 K in the same feed gradually shifted Pd peaks, and the XRD signal clearly differed from the previous scans at room temperature. Heat was stopped after holding for 30 min at 393 K, and a long scan was conducted in He (Figure 2a); the full range of Figure 2a is displayed in Figure S4 in the Supporting Information). Subsequently, to investigate the entirety of the new phase formation, another long scan at room temperature was performed in the presence of 4% H_2 . Since no change was detected (Figure S5 in the Supporting Information), we conclude that the shifted phase formation was complete within the detection limit, because the rest of Pd would respond with H_2 . Crystallite size determined from the XRD peak profile showed no difference between fresh and heated samples, which indicate that the observed peak shifts were not caused by a sintering effect. The newly formed phase with a shifted peak is congruent with previous XRD studies of PdC_x formation under various hydrocarbon atmospheres.^[3–6,17–19]

In Figure²^b, the same series of in situ experiments were conducted under the same conditions for Pd/CNTs, and PdC_x phase transformation was observed until its saturation. Detailed XRD scans for Pd/CNTs in identical experimental stages are shown in Figures⁶⁻⁻⁹ in the Supporting Information. Compared with the Pd/CNTs, XRD signals for Pd/Al₂O₃ are lower at the same counting time because of high background patterns given by the Al₂O₃ support.

The morphologies of reacted samples in the in situ XRD chamber were studied by using electron microscopy. The TEM image in Figure³^a shows the Pd particle dispersion status with an average size distribution about 3 nm (in line with the peak calibration from XRD) on Al₂O₃ support. After a reaction under in situ conditions, remarkable changes in the catalyst morphology can be clearly seen from Figure³^b and c. Carbonaceous species deposited heavily on Pd particles and the Al₂O₃ support. TEM observation and EDX mappings display the deposition degree that generated carbon species possess an even larger volume than the Al₂O₃ support. Clearly, the porous structures of Al₂O₃ are covered by carbon deposition in micron scales, thus, contact routes to embedded Pd nanoparticles were blocked. Moreover, pulled-out Pd nanoparticles were also observed along the edges of deposited carbons. This can explain the observation that Pd signals dispersed in line with carbon and oxygen, but not aluminum in the EDX mapping (Figure³^c). More microscopic results are shown in Figures¹⁰ and ¹¹ in the Supporting Information. Observation in high resolution was attempted, but a clear image of Pd nanoparticles and Al₂O₃ support were unobtainable due to the heavy coverage of carbon deposition on the catalysts surface. The observed morphology on reacted Pd/Al₂O₃ illustrates Pd particle movement in the way that deposited carbon species pulled out Pd particles from the support and carried them during its accumulation.

Similar to the case of Pd/CNTs, carbonaceous deposition was also observed on a reacted sample when compared with fresh one (fresh Pd/CNTs is shown in Figure⁴^a). However, the carbon deposit, primarily formed on the surface of Pd particles, migrated onto the surface of CNTs (Figure⁴^b--f). Interactions between functionalized CNTs and metal particles prevent metal particle sintering and permit a good


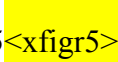
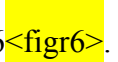
dispersion of nanoscale particles on CNTs.^[20] In addition, as one-dimensional, hollow structural materials, CNTs have large planar surfaces on their outer surfaces and inner cavities.^[21,22] Therefore, continuously migrated carbonaceous species are invited to spread without encountering kinks or obstacles due to the SMSI effect. As a result, carbonaceous species act as bridges connecting Pd particle islands on CNT walls (Figure^{4d} and e). As for the individual Pd particles on CNT, certain surfaces are clearly accessible with the carbonaceous deposition migrated onto the vicinity of CNT surfaces (Figure^{4b} and c). Figure^{4f} shows an end of CNT that remained open while accumulated deposition continuously migrated into inner cavity of the CNT. In addition to Figure⁴, a local area with dispersed Pd nanoparticles is shown in Figure^{S12} in the Supporting Information, in which the overview morphology shows a much less carbonaceous deposition compared with Pd/Al₂O₃ due to its migration on CNT surfaces.

Because the electrical modification achieved stabilization due to the saturation of the PdC_x phase, observed morphology differences between reacted Pd/Al₂O₃ and Pd/CNTs arouses practical and technical interest in the activity and selectivity for further catalytic tests in the acetylene-hydrogenation flow reactor. Elevated conditions with an ethylene-rich feed were utilized for simulating industrially-applied, acetylene-selective hydrogenation conditions. As shown in Figure⁵, after 16.5 h on stream, the conversion for Pd/Al₂O₃ dropped to 50% and selectivity held at 20% (Figure^{5a}). Surprisingly for Pd/CNTs, conversion remained at 80% and selectivity was 35% (Figure^{5b}). Carbon monoxide chemisorption (for detection parameters, see the Supporting Information) determines the specific Pd surface area and permits the calculation of activities per "surface Pd" for Pd/Al₂O₃ ($433 \text{ g} \langle \text{C}_2\text{H}_2 \rangle / \text{m}_{\text{Pd}}^{<M-2> \text{h}^{<M-1>}}$) and Pd/CNTs ($2380 \text{ g} \langle \text{C}_2\text{H}_2 \rangle / \text{m}_{\text{Pd}}^{<M-2> \text{h}^{<M-1>}}$).

Before interpreting the catalytic data, it is worth stressing the difficulty of characterizing reacted catalysts in the flow reactor due to the microscale weight of usages and highly diluted existences (usages: 0.08 mg Pd/CNTs and 0.1 mg Pd/Al₂O₃, both were diluted by using 100 mg boron nitride). Therefore, in situ analyses were introduced to interpret the role of the PdC_x phase during hydrogenation test. Detailed experimental

parameters are considered to bridge the differences between in situ and flow-reactor conditions. First, the weight hourly space velocities (WHSV) of hydrocarbon on both catalysts are higher under flow-reactor conditions (112.5 $\text{L} \cdot \text{g}^{-1} \cdot \text{h}^{-1}$ of C_2H_2 and 11250 $\text{L} \cdot \text{g}^{-1} \cdot \text{h}^{-1}$ of C_2H_4 for Pd/CNTs and 90 $\text{L} \cdot \text{g}^{-1} \cdot \text{h}^{-1}$ of C_2H_2 and 9000 $\text{L} \cdot \text{g}^{-1} \cdot \text{h}^{-1}$ of C_2H_4 for Pd/ Al_2O_3) than in in situ conditions (4 $\text{L} \cdot \text{g}^{-1} \cdot \text{h}^{-1}$ of C_2H_2 for both catalysts). Second, ratios of partial pressures between hydrocarbon and hydrogen are higher in flow reactor ($\text{C}_2\text{H}_4/\text{H}_2$ 10:1) than in situ conditions ($\text{C}_2\text{H}_2/\text{H}_2$ 1:2). Third, higher temperature was applied in flow reactor than in situ conditions. Due to the physical, chemical, and thermal properties of PdC_x phase formation,^[6,7] every condition applied in flow-reactor conditions favored earlier saturations of PdC_x compared with in situ conditions.

. In the present work, confirming the physical saturation of PdC_x in the beginning of hydrogenation discriminates and stabilizes the reaction-active phase by displaying the same carbon concentrations in subsurface and surface regions for both catalysts. Thus, subsurface PdC_x , in this work, is not a dynamic factor for observed differences in catalytic results.

Simplifying reactive complexity promotes a better understanding of the reaction pathway; herein, stabilizing the reaction-active phase led to a straightforward approach by using the observed morphology differentiation (the SMSI effect) as the controlling factor for reading catalytic performance. A mechanism sketch, based on obtained evidences and analyses illustrated in Figures⁴  and 5 , is shown in Figure⁶ . In the beginning of the acetylene-hydrogenation process, the Pd surface is immediately covered by dissociatively adsorbed carbon species. Simultaneously, adsorbed carbon is gradually incorporated into the Pd lattice, and acetylene-derived oligomers start to deposit on Pd and support surfaces. The CNTs' opened ends, straight walls and regular cavities permit the migration of coke deposition and regular exposure of saturated PdC_x . Similar to the case of Pd/ Al_2O_3 , due to the irregular porous structures with smaller diameters, deposited species encounter kinks and obstacles and accumulate into large surface oligomers/polymers. The appearance of lifted Pd particles along the edge of deposited layers proves the diffusion limit for accumulated species and the dynamic movement of Pd on Al_2O_3 . As a consequence, the exposure of the reaction-selective PdC_x phase was limited by overwhelmed coverage of

accumulated carbon layers. Other factors would also possibly affect obtained difference in selectivity, for example, the Pd particle size and support acidity. However, in situ studies in present work revealed that the electrical and structural modifications of Pd nanoparticles under reaction conditions were not influenced by particle size and acidities of the supporting material. .<?><?>change ok?<?><?>

The present work targets three long-overlooked facts. First, forming subsurface PdC_x by diffusing carbon atoms into a Pd lattice is irrelevant to particle size and supporting materials. Second, subsurface PdC_x cannot be discussed as the single impact factor affecting a reaction, because the carbon concentration in PdC_x is determined by the level of carbon diffusion. If it obtains saturation, subsurface PdC_x on different supports influences the reaction indiscriminately, because the carbon concentrations are identical. Finally, the saturation of the PdC_x phase is a physical process, which happens irreversibly at the beginning of contact with hydrocarbon or under hydrogenation reactions. Saturated PdC_x governs the electronic properties of modified Pd by dominating subsurface chemistry.

Establishing a relationship between in situ and simulated industrial conditions contributes to a better understanding of stabilizing subsurface chemistry by ensuring the saturation process of PdC_x. Onwards, carbonaceous deposition interacts with PdC_x and co-catalyzes selective hydrogenation. Due to the absence of metallic Pd, rearrangement of deposited species on support surface and exposing catalytically selective sites on the PdC_x surface can improve the selectivity toward ethylene. Without promoters and alloying with other elements, results in this work may enlighten the design methodology of transition-metal-supported catalyst systems, because current strategy simplifies the active complex during reactions and offers a possibility to control catalytically active centers by: 1) saturating the active transition metal and forming stable, but selective phases in the beginning of hydrogenation; 2) choosing supports with suitable geometric structures; and 3) establishing an SMSI effect to regularly rearrange accumulated species and expose the reaction-active phase.

Experimental Section

PR24-LHT carbon nanotubes were purchased from Pyrograf Products Inc. (Ohio, USA). Concentrated nitric acid (70%, Sigma--Aldrich) was used to functionalize CNTs at 383 K for 4 h. Pd/CNTs was prepared in the following route: 34.1 mg palladium nitrate ($\approx 40\%$ Pd, Roth) was dissolved in ethanol (80 mL). Functionalized CNTs (300 mg) were then mixed in the solution. Ultrasonication was carried out for one hour and followed by evaporation at RT. Sample was then collected and calcinated in air at 250 °C. Reduction was conducted in 25% H₂ mixed with He in a total flow of 100 mL min⁻¹ at 823 K. Pd/Al₂O₃ catalyst is commercially available from Sigma--Aldrich (5 wt%, 50--180 μm).

Catalysis measurements were conducted in a feed (30 mL min⁻¹) of 0.5% C₂H₂, 5% H₂ (99.999%), and 50% C₂H₄ (99.95%) in helium (99.999%). For more experimental details, see the Supporting Information.

Acknowledgements

We thank Dr. Malte Behrens, Dr. Dirk Rosenthal, and Dr. Olaf Timpe for discussions, Dr. Marc Armbrüster and Matthias Friedrich for the technical assistance of the catalytic test. D.S.S. thanks the financial support from MOST (2011CBA00504) and NSFC (50921004, 20973079, 21133010) of China.

<lit1><jnl>G. C. Bond, D. A. Dowden, N. Mackenzie, *Trans. Faraday Soc.* **1958**, *54*, 1537</jnl>.

<lit2><book>G. Webb in *Comprehensive Chemical Kinetics*, Vol. 20 (Eds.: C. H. Bamford, C. F. H. Tipper), Elsevier, Amsterdam, **1978**, p. 1</book>.

<lit3><jnl>D. Teschner, Z. Révay, J. Borsodi, M. Hävecker, A. Knop-Gericke, R. Schlögl, D. Milroy, S. D. Jackson, D. Torres, P. Sautet, *Angew. Chem.* **2008**, *120*, 9414; *Angew. Chem. Int. Ed.* **2008**, *47*, 9274</jnl>.

<lit4><jnl>D. Teschner, J. Borsodi, A. Wootsch, Z. Revay, M. Havecker, A. Knop-Gericke, S. D. Jackson, R. Schlögl, *Science* **2008**, *320*, 86</jnl>.

<lit5><jnl>A. Frąckiewicz, A. Janko, *Acta Cryst* **1978**, *A34*, 377</jnl>.

- <lit6><jnl>J. Stachurski, A. Frackiewicz, *J. Less-Common Met.* **1985**, *108*, 249</jnl>.
- <lit7><jnl>J. Stachurski, *J. Chem. Soc. Faraday Trans.* **1985**, *81*, 2813</jnl>.
- <lit8><jnl>A. Borodziński, *Polish. J. Chem.* **1998**, *72*, 2455</jnl>.
- <lit9><jnl>A. S. Al-Ammar, G. J. Webb, *J. Chem. Soc. Faraday Trans. 1* **1978**, *74*, 657</jnl>.
- <lit10><jnl>A. Borodziński, *Catal. Lett.* **1999**, *63*, 35</jnl>.
- <lit11><jnl>K. M. Neyman, S. Schauermaun, *Angew. Chem.* **2010**, *122*, 4851; *Angew. Chem. Int. Ed.* **2010**, *49*, 4743</jnl>.
- <lit12><jnl>M. Wilde, K. Fukutani, W. Ludwig, B. Brandt, J.-H. Fischer, S. Schauermaun, H. J. Freund, *Angew. Chem.* **2008**, *120*, 9430; *Angew. Chem. Int. Ed.* **2008**, *47*, 9289</jnl>.
- <lit13><jnl>S. J. Tauster, S. C. Fung, R. T. K. Baker, J. A. Horsley, *Science* **1981**, *211*, 1121</jnl>.
- <lit14><jnl>A. Rinaldi, J.-P. Tessonnier, M. E. Schuster, R. Blume, F. Girgsdies, Q. Zhang, T. Jacob, S. B. A. Hamid, D. S. Su, R. Schlögl, *Angew. Chem.* **2011**, *123*, 3371; *Angew. Chem. Int. Ed.* **2011**, *50*, 3313</jnl>.
- <lit15><jnl>M. C. Burrell, G. A. Smith, J. Chera, *J. Surf. Inter. Anal.* **1988**, *11*, 160</jnl>.
- <lit16><jnl>D. Teschner, E. Vass, M. Havecker, H. Sauer, A. Knop-Gericke, R. Schlögl, J. McGregor, L. F. Gladden, *J. Catal.* **2006**, *242*, 26</jnl>.
- <lit17><jnl>S. B. Ziemecki, G. A. Jones, D. G. Swartzfager, R. L. Harlow, J. Faber, *J. Am. Chem. Soc.* **1985**, *107*, 4547</jnl>.
- <lit18><jnl>S. B. Ziemecki, G. A. Jones, *J. Catal.* **1985**, *95*, 621</jnl>.
- <lit19><jnl>S. B. Ziemecki, G. A. Jones, D. G. Swartzfager, *J. Less-Common Met.* **1987**, *131*, 157</jnl>.

<lit20><jnl>L.[^]D. Shao, W. Zhang, M. Armbrüster, D. Teschner, F. Girgsdies, B. Zhang, O. Timpe, M. Friedich, R. Schlögl, D.[^]S. Su, *Angew. Chem.* **2011**, *123*, 10414; *Angew. Chem. Int. Ed.* **2011**, *50*, 10231</jnl>.

<lit21><jnl>S. Iijima, *Nature* **1991**, *354*, 56</jnl>.

<lit22><jnl>L.[^]D. Shao, T.[^]W. Lin, G. Tobias, M.[^]L.[^]H. Green, *Chem. Commun.* **2008**, 2164</jnl>.

Received: July 24, 2012

Published online on <?><?>

Figure[^]1 In situ XPS investigations: Pd 3d 5/2 region of Pd/CNTs by using 720[^]eV photon energy measured in the a)[^]"as is" state and b)[^]under C₂H₂ hydrogenation.

Figure[^]2 In situ XRD investigations under hydrogen and reaction conditions (2[^]% C₂H₂, 4[^]% H₂, rest in He in total flow of 100[^]mL[^]min[^]⁻¹) over Pd/Al₂O₃ and Pd/CNTs, both in 30[^]mg: a)[^]Pd/Al₂O₃, fresh sample (black), recorded under H₂ (red), recorded under reaction conditions heated up to 393[^]K (blue); b)[^]Pd/CNT, fresh sample (black), recorded under H₂ (red), recorded under reaction conditions heated up to 393[^]K (blue). XRD patterns refer to: Pd (PDF card 46-1043); PdH (PDF card 18-0951); Al₂O₃ (PDF card 29-0063).

Figure[^]3 Microscopic observations of a)[^]fresh Pd/Al₂O₃, b) and c)[^]recorded after in situ XRD investigations.

Figure[^]4 Microscopic observations of a)[^]fresh Pd/CNTs, b),[^]c),[^]d),[^]e), and f)[^]recorded after in situ XRD investigations.

Figure[^]5 Conversion (<?kv>) and selectivity (<?kl>) during acetylene hydrogenation on a)[^]0.1[^]mg Pd/Al₂O₃ and b)[^]0.08[^]mg Pd/CNTs carried out with isothermal experiments at 473[^]K with a feed of 0.15[^]mL[^]min[^]⁻¹ C₂H₂, 1.5[^]mL[^]min[^]⁻¹ H₂, and 15[^]mL[^]min[^]⁻¹ C₂H₄.

Figure[^]6 Scheme of carbonaceous deposition on Al₂O₃ and CNTs simulated from observed microscopic results in Figures[^]3<xfigr3> and 4<xfigr4>.